Wave propagation in reinforced and prestressed concrete structures with damage

E. El Masri [1], **N. Ferguson** [1], **T. Waters** [1]
[1] Institute of Sound and Vibration Research, University of Southampton,
Southampton, SO17 1BJ, UK
e-mail: **eem3g14@soton.ac.uk**

Abstract
Corrosion of the steel reinforcement bars in reinforced concrete is the most common cause of premature failure that must be pre-empted. In this respect, wave based techniques provide a potential detection approach. In this paper, wave propagation is modelled in a steel reinforced concrete beam with and without prestress. A short section of the beam is modelled in ANSYS. This model is then used in the wave finite element (WFE) framework, which assumes spatial periodicity along the waveguide, to model a beam of infinite extent. Corrosion of the reinforcement bars is represented by a local loss of thickness. Numerical case studies are presented to investigate the effects of various configurations and the severity of damage on the dispersion curves of the propagating waves. Scattering matrices are also calculated for the damage site, by coupling damaged and undamaged sections of the waveguide. Wave modes are subsequently identified for which the reflection coefficients are potentially sufficiently large to observe and use for damage identification.

1 Introduction

Most damage in reinforced concrete structures comprising steel bars is due to corrosion and delamination. Before any repair procedures can take place, this damage should be located and quantified. Because the repair and maintenance costs are considerable, an early detection of damage is needed. The majority of non-destructive techniques (NDT) require knowledge of the existence of the deterioration. Thus, vibration based methods have been developed as both global and local approaches to detect damage. These methods can be divided into modal and wave based methods. In the latter, knowledge of the wave characteristics is essential within a specified waveguide. Since the structure is a composite, analytical solutions do not exist and a numerical approach is needed. One approach to analyse a waveguide is the spectral finite element (SFE). However, this method requires new spectral mass and stiffness matrices for each scenario on a case-by-case basis [1]. Alternatively, the Wave Finite Element method (WFE) can adopted, where a small segment of the waveguide is modelled via FE. By applying periodicity, the free and forced wave propagation problems can be solved for a uniform waveguide whose cross section is defined by modelled section.

Mace and Duhamel presented the WFE method for simple homogeneous one dimensional waveguides. The efficiency and accuracy of this method was compared to the spectral FE method for predicting the free and forced response for a beam, a simply supported plate strip and a viscoelastic laminate [2, 3]. Mencik and Ichchou formulated and solved for wave propagation in guided elastodynamic structures filled with acoustic fluid using WFE. Free and forced responses of the waveguide were presented, and comparisons between the proposed method and classical theories were formulated showing that this method is not limited to low frequencies [4]. In a later application, Waki *et al.* expressed free and forced vibrations of a tyre using the WFE formulation on a short circumferential segment, and results were compared to experiments [5]. In addition, they considered numerical issues concerning the wave finite element method for free and forced vibrations of waveguides, and a robust procedure was proposed. There are many examples covering free

wave propagation in an Euler Bernoulli beam and a thin plate strip [6]. Renno and Mace formulated a rectangular segment as a waveguide via WFE. Then, the forced response to a convected harmonic pressure (CHP) was formulated, where a comparison was presented between FE and WFE predictions of a frequency response function for a cantilever-laminated beam [1]. Furthermore, they calculated the forced response of two-dimensional homogeneous media via WFE. Numerical examples covered isotropic, orthotropic and laminated plates [7]. Zhou *et al.* compared wave propagation results between the semi-analytical finite element (SAFE) method and WFE for a steel pipe. Efficiency and accuracy of both methods were examined [8].

One of the major advantages of the WFE method is in coupling damaged and undamaged waveguides to predict the reflection and transmission coefficients due to a defect. For instance, Renno and Mace calculated the reflection and transmission coefficients of joints using a hybrid wave finite element approach, where the joint is modelled via FE and a small portion of the waveguide is expressed via WFE. Forced response examples were presented for two rods connected at a point mass, an L-frame configuration, and lap-jointed laminated beams with a slot [9]. Ichchou et al. applied the WFE method to obtain the wave mode shapes and forced response for a rectangular cross section waveguides. The diffusion matrix prediction model (DMM) was used to couple damaged and undamaged waveguides, where higher modes show sensitivity to damage modelled as a notch within the section [10]. In addition, Zhou and Ichchou expressed wave excitation and scattering using the eigensolutions from WFE of coupled structures comprising damaged and undamaged plates [11]. Later, they used the WFE method to obtain the wave characteristics of a curved beam. Mode conversion and reflection and transmission coefficients were used to localize the damaged portions [12]. Subsequently, Kharrat proposed the identification and sizing of defects in pipelines by the wave finite element method using torsional guided waves. Reflections from cracks were used to quantify the extent of damage. WFE was applied to predict the wave characteristics of hollow cylinders, and good agreement was found with respect to a full finite element simulation [13]. In addition, Kharrat *et al.* used WFE to construct a numerical database of reflection coefficients by varying the dimensions of damage in pipelines. Torsional guided waves were also proposed for pipeline inspection [14]. Furthermore, Kessentini *et al.* calculated the scattering coefficients of coupling elements using WFE solutions in order to illustrate the forced response to pressure excitations with and without the effect of damping [15].

In this paper, WFE is applied to a reinforced deep concrete beam section with and without prestress. Dispersion curves and mode shapes are plotted for the least attenuated waves. Then, reflection coefficients associated with the presence of a damaged section are computed to inspect and comment upon their sensitivity to an introduced defect representing the corrosion of a steel rebar.

2 WFE formulation

The WFE concept predicts the wave characteristics of a structure through analysing the wave propagation within a short section of the waveguide. By expressing the continuity of displacements and equilibrium of forces at the boundaries between successive segments, an eigenvalue problem is posed in terms of a transfer function across the section. The eigenvalues obtained relate the variables associated with the right and left sides of the section, and are a function of the wavenumbers for the waveguide. In addition, the eigenvectors are associated with the displacements and forces on the cross section of the boundaries. This problem is solved at each specified frequency.

The length of the section of the waveguide modelled, Δ, should not be too small with respect to the shortest wavelength to avoid round-off errors, nor too large to reduce discretization errors [6]. The dynamic stiffness matrix is then developed using the mass and stiffness matrices. Commercial FE packages are used to model the waveguide section and to extract the required matrices. In this paper, ANSYS is used to model the reinforced waveguide section. After extracting the mass and stiffness matrices, the dynamic stiffness matrix is manipulated to formulate the transfer matrix, and then the eigen problem is solved to obtain the wavenumbers and wave mode shapes at each frequency of interest. The key expressions and relationships

are given briefly below. The dynamic stiffness matrix at frequency ω of a finite section of waveguide relating the element nodal displacements and forces is given by

$$\mathbf{D} = \mathbf{K} - \omega^2 \mathbf{M} \tag{1}$$

where $\mathbf{K}$ and $\mathbf{M}$ are the $N \times N$ stiffness and mass matrices of the waveguide section, where N is the total number of DOFs . L and R denote the left and right sides as in Figure 1. The dynamic stiffness matrix is partitioned accordingly,

$$\begin{bmatrix} \boldsymbol{D_{LL}} & \boldsymbol{D_{LR}} \\ \boldsymbol{D_{RL}} & \boldsymbol{D_{RR}} \end{bmatrix} \begin{bmatrix} \boldsymbol{q_L} \\ \boldsymbol{q_R} \end{bmatrix} = \begin{bmatrix} \boldsymbol{f_L} \\ \boldsymbol{f_R} \end{bmatrix} \tag{2}$$

The periodic conditions for the displacements and the equilibrium condition at the junction of the two elements are $\boldsymbol{q_R}$=$\lambda \boldsymbol{q_L}$ and $\boldsymbol{f_R}$=-$\lambda \boldsymbol{f_L}$ where the propagation constant $\lambda = e^{-ik\Delta}$ relates the right and left displacements and forces, and k is the wavenumber. Equation (2) can be rearranged and written as

$$\mathbf{T} \begin{Bmatrix} \boldsymbol{q_L} \\ \boldsymbol{f_L} \end{Bmatrix} = \lambda \begin{Bmatrix} \boldsymbol{q_L} \\ \boldsymbol{f_L} \end{Bmatrix} \tag{3}$$

The transfer function matrix $\mathbf{T}$ must ensure continuity of displacements $\boldsymbol{q}$ and equilibrium of forces $\boldsymbol{f}$ between the boundaries of two consecutive elements [2]. It is expressed as

$$\mathbf{T} = \begin{bmatrix} -\boldsymbol{D_{LR}^{-1}} \boldsymbol{D_{LL}} & \boldsymbol{D_{LR}^{-1}} \\ -\boldsymbol{D_{RL}} + \boldsymbol{D_{RR}} \boldsymbol{D_{LR}^{-1}} \boldsymbol{D_{LL}} & -\boldsymbol{D_{RR}} \boldsymbol{D_{LR}^{-1}} \end{bmatrix} \tag{4}$$

The transfer matrix eigenvalue problem is solved at each frequency step, where the wavenumbers k are related to the eigenvalues. The positive-going waves are characterized by $\left|\lambda_j^+\right| < 1$ and the negative-going waves by $\left|\lambda_j^+\right| > 1$. However, for $\left|\lambda_j^+\right| = 1$, the associated waves are considered positive-going if they fulfil the condition $Re\left\{\boldsymbol{f_L^H} \dot{\boldsymbol{q}}_{\boldsymbol{L}}\right\} = Re\left\{i\omega \boldsymbol{f_L^H} \boldsymbol{q_L}\right\} < 0$. Furthermore, the wave modes associated with the right eigenvectors of Equation(3) are grouped into positive and negative-going waves

$$\boldsymbol{\Phi}^+ = [\boldsymbol{\Phi}_1^+ \cdots \boldsymbol{\Phi}_N^+] \;\; ; \;\; \boldsymbol{\Phi}^- = [\boldsymbol{\Phi}_1^- \cdots \boldsymbol{\Phi}_N^-] \;\; ; \;\; \boldsymbol{\Phi} = [\boldsymbol{\Phi}^+ \quad \boldsymbol{\Phi}^-] \tag{5}$$

where each wavemode is divided into displacement $\boldsymbol{q}$ and force $\boldsymbol{f}$ sub-vectors, i.e.

$$\boldsymbol{\Phi}_j = \begin{Bmatrix} \boldsymbol{\Phi_q} \\ \boldsymbol{\Phi_f} \end{Bmatrix}_j \tag{6}$$

One can obtain the left eigenvectors of the transfer matrix $\mathbf{T}$ as well. They can be partitioned and grouped as follows

$$\boldsymbol{\Psi}_j = \begin{Bmatrix} \boldsymbol{\Psi_f} & \boldsymbol{\Psi_q} \end{Bmatrix}_j \;\; ; \;\; \boldsymbol{\Psi}^{\pm} = \begin{bmatrix} \boldsymbol{\Psi}_1^{\pm} \\ \cdots \\ \boldsymbol{\Psi}_N^{\pm} \end{bmatrix} \;\; ; \;\; \boldsymbol{\Psi} = \begin{bmatrix} \boldsymbol{\Psi}^+ \\ \boldsymbol{\Psi}^- \end{bmatrix} \tag{7}$$

The left and right wavemodes are orthogonal, and can be normalised so that

$$\boldsymbol{\Psi}^+ \boldsymbol{\Phi}^+ = \mathbf{I} \tag{8}$$

A useful consequence of this normalisation is to improve conditioning of matrices that must be inverted [6].This can be accomplished by premultiplying the intended matrix by the normalised right eigenvectors. Furthermore, the transformations between the physical domain, where the motion is described in terms of $\boldsymbol{q}$ and $\boldsymbol{f}$, and the wave domain, where the motion is described in terms of waves of amplitudes $\mathbf{a}^+$ and $\mathbf{a}^-$ travelling in the positive and negative directions respectively, are accomplished via

$$\begin{Bmatrix} \boldsymbol{q_L} \\ \boldsymbol{f_L} \end{Bmatrix} = \begin{bmatrix} \boldsymbol{\Phi_q^+} & \boldsymbol{\Phi_q^-} \\ \boldsymbol{\Phi_f^+} & \boldsymbol{\Phi_f^-} \end{bmatrix} \begin{Bmatrix} \mathbf{a}^+ \\ \mathbf{a}^- \end{Bmatrix} \tag{9}$$

The rapidly decaying wavemodes are removed due to their negligible contributions to the far field response, which can otherwise cause ill-conditioning problems [6]. Thus, only m pairs of positive and negative going waves are retained based on a user-defined criterion at each frequency step. As a result, the size of the model will be smaller, and calculation time is reduced.

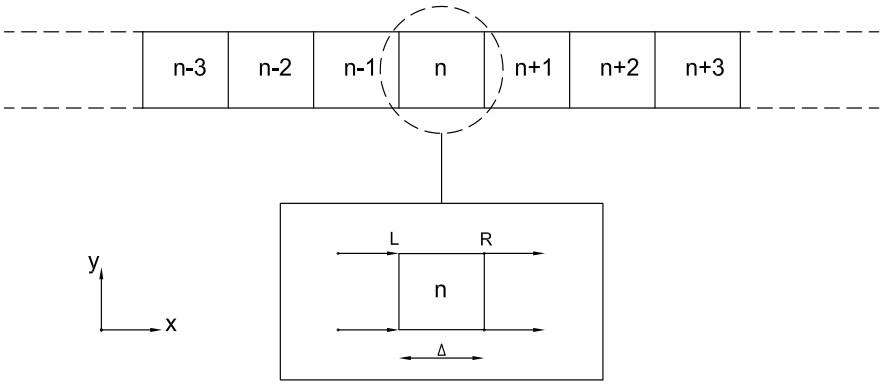

Figure 1: Structure with periodic elements. A cell of length Δ is shown with the force and displacement vectors on the right and left-hand sides

3 Reinforced concrete and prestressed reinforced concrete modelling in ANSYS

In order to apply the WFE method to a reinforced concrete beam, a section needs to be modelled in ANSYS in order to extract the associated mass and stiffness matrices. Concrete is modelled using the SOLID65 element which is a 3D solid element. It has three DOFs, which are translations in the X, Y and Z directions, and it is defined by eight nodes. Reinforcement rebars are modelled via the 3D discrete element REINF264 embedded in the SOLID65 element. The nodal locations, degrees of freedom and connectivity of the REINF264 element are identical to those of the base element which is the SOLID65 [16].The location of the rebar is defined as an offset distance from the edges of the base element selected.

The undamaged reinforced concrete section is modelled using 16 SOLID65 elements, with the dimensions and properties shown in Figure 2 and Table 1. The total number of DOFs *N* is 150 for this model. The damaged reinforced concrete section is modelled in the same way as for the undamaged section, except that the area of the damaged reinforced rebar at the bottom right corner is reduced to represent a loss of thickness due to corrosion. In this model, the corroded rebar is taken to have a diameter equivalent to a 60 percent reduction compared to the intact one.

Prestressed concrete is a type of reinforced concrete in which at least part of the steel reinforcement has been tensioned against the concrete. In the pretensoning system, steel rods or tendons (individual wires or strands) are first tensioned on a casting bed using jacks, and then concrete is poured as shown in Figure 3. The prestressed RC section is first modelled in ANSYS using SOLID65 elements for concrete and REINF264 as embedded reinforcement similar to the conventional RC section. The prestressing effect is modelled via an initial strain in the tendon elements, corresponding to tendon tensile forces, in a preliminary load stage. The initial strain value is calculated based on steel reinforcement material properties and the prestress force applied. Also, one can assume that the tension prestress force of the steel reinforcement is equal to 70 percent of its ultimate tensile strength ($0.4\times10^9 Pa$). This force is used to prestress both damaged and undamaged rebars. Thus, the stress value used to calculate the initial strain for the damaged rebar is higher than the undamaged one since the cross sectional area is smaller for the same amount of prestress force. Subsequently, $\varepsilon_1 = 0.0014$ and $\varepsilon_2 = 0.0036$ are the initial strain values for the undamaged and damaged rebars respectively. In this model, the damaged reinforcement includes one of the rebars where the strain values are assigned. The section details of damaged and undamaged prestressed RC, and material properties are similar to those of conventional RC model defined before.

The mass and stiffness matrices were extracted using ANSYS software for both the damaged and undamaged segments of RC and prestressed RC, and then post-processed using WFE. There are 150 different wavenum-

bers in accordance with number of DOFs, but most of them have a significant imaginary part corresponding to highly attenuated waves, and therefore need to be eliminated. In these models, only the wave modes associated with $|Im\,(k\Delta)| \leq 0.3$ are retained at each frequency step. This corresponds to an attenuation of 10 dB along the element length in the direction of propagation.

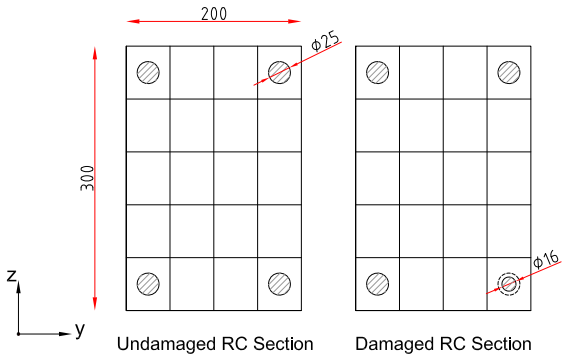

Figure 2: Undamaged and damaged RC section details

Properties	**Concrete**		**Steel**	
Dimensions	Length of element Δ (m)	0.01	Rebar area (m^2)	0.00051
	Length in y-direction (m)	0.2	-	-
	Length in z-direction (m)	0.3	-	-
Material	Young Modulus (Pa)	25×10^9	Young Modulus (Pa)	200×10^9
	Poisson ratio ν	0.18	Poisson ratio ν	0.3
	Density ρ (kg/m^3)	2400	Density ρ (kg/m^3)	7850

Table 1: Dimensions and material properties of concrete and steel materials

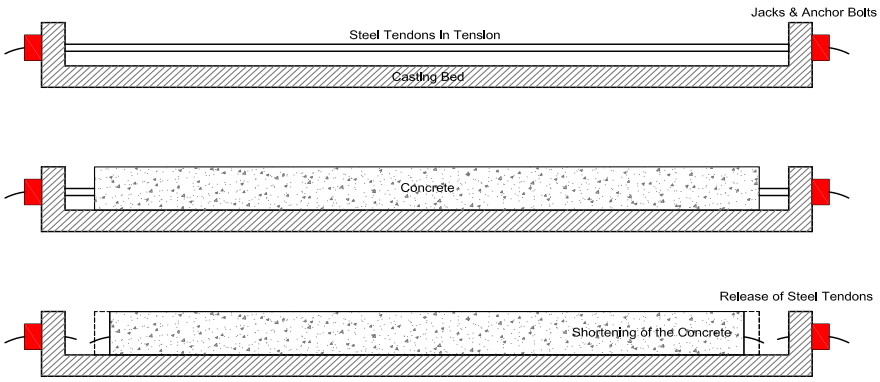

Figure 3: Procedure for prestressing reinforced concrete [17]

4 Dispersion relations of prestress RC

The wave modes are evaluated within the frequency range of 1 to 15 kHz with a frequency step of 50 Hz. The dispersion curves relating to the least attenuated waves are plotted for both the damaged and undamaged

waveguides. These modes are divided into three categories. Zero order modes are the ones that can propagate over the whole frequency band, evanescent modes are the ones with purely imaginary wavenumbers before their cut-on frequency, and complex modes are the ones with complex wavenumbers before their cut-on frequency. Above cut-on, the wavenumber becomes purely real for both evanescent and complex modes. Figure 4 presents the dispersion curves for zero order modes. Only the real part of these wavenumbers is plotted, since with no damping in the model the imaginary part is zero. Mode 1 is associated with axial motion, mode 2 with torsional around the x-axis, and modes 3 and 4 with bending in the vertical and transverse directions respectively. In addition, Figures 5 and 6 present the dispersion curves of the waves that are evanescent and complex respectively. Dispersion curves for RC and prestressed RC are similar for zero order modes, but differ for evanescent and complex modes. In this paper, only the dispersion curves for prestressed RC are plotted. In all cases, only slight changes are observed between the wavenumbers of the damaged and undamaged waveguides. This due to the fact that the structural stiffness is governed by the concrete rather than by the reinforcement rebars.

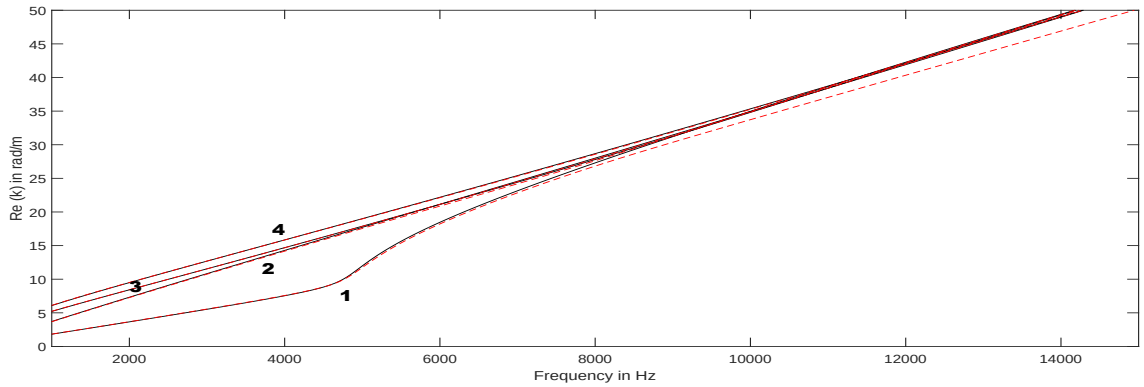

Figure 4: Real part of the wavenumbers of prestressed RC for zero order wave modes: Undamaged section (—), Damaged section (- - -)

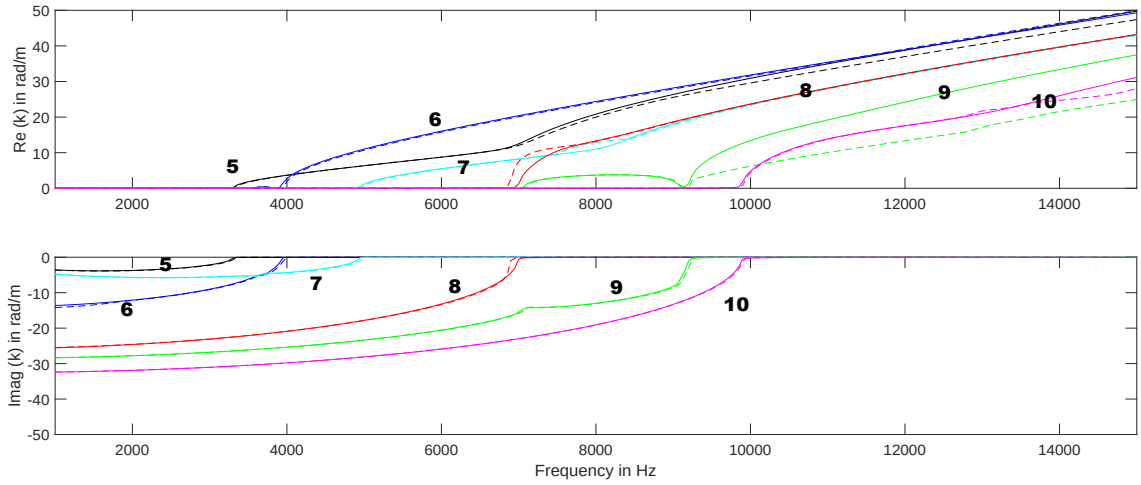

Figure 5: Real and imaginary parts of the wavenumbers of prestressed RC for evanescent wave modes: Undamaged section (—), Damaged section (- - -)

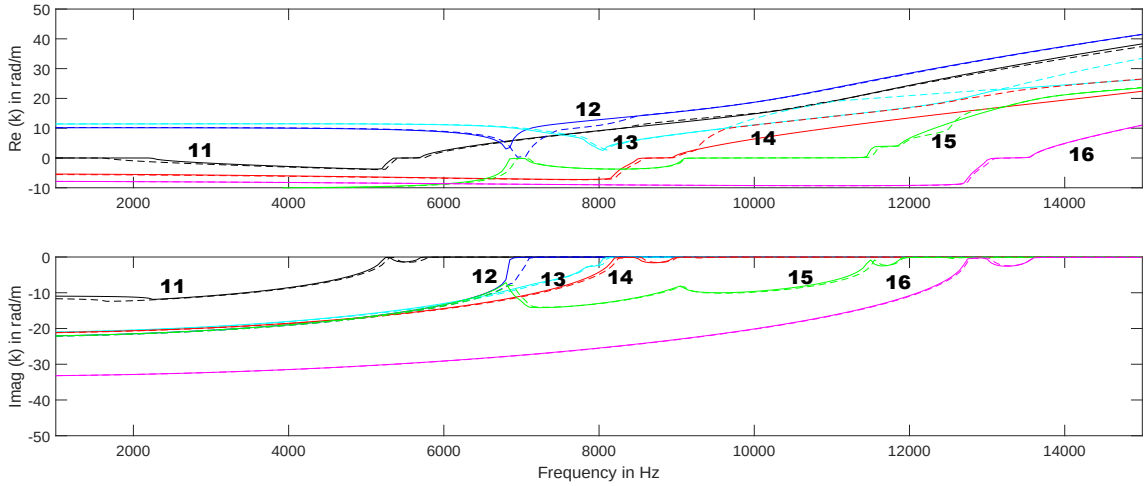

Figure 6: Real and imaginary parts of the wavenumbers of prestressed RC for complex wave modes: Undamaged section (—), Damaged section (- - -)

5 Coupling approach using WFE-FE-WFE

Damage or discontinuities in structures give rise to scattering of incident waves, which is potentially of use for damage inspection. One can model the damaged and undamaged waveguides as two semi-infinite beams, and couple the waves at the interface of the junction. This model is denoted here as the WFE-WFE approach. When considering the total scattering caused by a discontinuity for finite length, coupling of a finite damage section to undamaged waveguides is a more appropriate model. In this case, a WFE-FE-WFE coupling approach can be used [9] and it is adopted here. The setup of the WFE-FE-WFE approach is shown in Figure 7.

In this model, the damaged section for the numerical simulations is modelled via FE of a finite length h = 0.05m of a segment length of Δ_i= 0.01m for both RC and prestressed RC models. Then, it is connected at each end to undamaged waveguide that is modelled using the WFE method as explained earlier. However, both interfaces are compatible since they have the same nodal meshes and DOFs. Let $\mathbf{D}_c$ be the dynamic stiffness matrix of the coupling joint, which is given in terms of its mass $\mathbf{M}_c$ and stiffness $\mathbf{K}_c$ matrices as follows [15]

$$\mathbf{D}_c = \mathbf{K}_c - \omega^2 \mathbf{M}_c \tag{10}$$

The left and right interface nodes of the coupling joint are expressed by l and r respectively. Internal nodes are denoted by i. $\mathbf{D}_c$ can be defined as

$$\mathbf{D}_c = \begin{bmatrix} \mathbf{D}_{ll} & \mathbf{D}_{li} & \mathbf{D}_{lr} \\ \mathbf{D}_{il} & \mathbf{D}_{ii} & \mathbf{D}_{ir} \\ \mathbf{D}_{rl} & \mathbf{D}_{ri} & \mathbf{D}_{rr} \end{bmatrix} \tag{11}$$

The dynamic stiffness matrix $\mathbf{D}_c$ of the coupling joint needs to be condensed into its internal DOFs using dynamic condensation presented in [6]. The condensed matrix is given as

$$\mathbf{D}_c^* = \begin{bmatrix} \mathbf{D}_{ll} - \mathbf{D}_{li}\mathbf{D}_{ii}^{-1}\mathbf{D}_{il} & \mathbf{D}_{lr} - \mathbf{D}_{li}\mathbf{D}_{ii}^{-1}\mathbf{D}_{ir} \\ \mathbf{D}_{rl} - \mathbf{D}_{ri}\mathbf{D}_{ii}^{-1}\mathbf{D}_{il} & \mathbf{D}_{rr} - \mathbf{D}_{ri}\mathbf{D}_{ii}^{-1}\mathbf{D}_{ir} \end{bmatrix} \tag{12}$$

The dynamic stiffness matrix $\mathbf{D}_c^*$ of the coupling joint relates the displacements and forces on its ends such that

$$\mathbf{D}_c^* \begin{Bmatrix} \boldsymbol{q}_l^c \\ \boldsymbol{q}_r^c \end{Bmatrix} = \begin{Bmatrix} \boldsymbol{f}_l^c \\ \boldsymbol{f}_r^c \end{Bmatrix} \tag{13}$$

Two coupled waveguide segments 1 and 2 belonging respectively to waveguides 1 and 2 are modelled via WFE. Let $\boldsymbol{a}^+, \boldsymbol{b}^-$ be the amplitudes of the waves incident on the coupling joint interface, and $\boldsymbol{a}^-, \boldsymbol{b}^+$ be the amplitudes of the waves reflected by the coupling joint interface. Vectors $\boldsymbol{q}$ and $\boldsymbol{f}$ are defined in the wave domain by Equation 9. For waveguides 1 and 2

$$\begin{Bmatrix} \boldsymbol{q}_r^1 \\ \boldsymbol{q}_l^2 \\ \boldsymbol{f}_r^1 \\ \boldsymbol{f}_l^2 \end{Bmatrix} = \begin{bmatrix} \boldsymbol{\Phi}_{\boldsymbol{q}_1}^+ & \mathbf{0} & \boldsymbol{\Phi}_{\boldsymbol{q}_1}^- & \mathbf{0} \\ \mathbf{0} & \boldsymbol{\Phi}_{\boldsymbol{q}_2}^+ & \mathbf{0} & \boldsymbol{\Phi}_{\boldsymbol{q}_2}^- \\ \boldsymbol{\Phi}_{\boldsymbol{f}_1}^+ & \mathbf{0} & \boldsymbol{\Phi}_{\boldsymbol{f}_1}^- & \mathbf{0} \\ \mathbf{0} & \boldsymbol{\Phi}_{\boldsymbol{f}_2}^+ & \mathbf{0} & \boldsymbol{\Phi}_{\boldsymbol{f}_2}^- \end{bmatrix} \begin{Bmatrix} \boldsymbol{a}^+ \\ \boldsymbol{b}^- \\ \boldsymbol{a}^- \\ \boldsymbol{b}^+ \end{Bmatrix} \tag{14}$$

where $\boldsymbol{\Phi}_{q,f}^+$ and $\boldsymbol{\Phi}_{q,f}^-$ are now defined by concatenating the relevant vectors for individual waveguides 1 and 2 after the application of WFE as follows

$$\boldsymbol{\Phi}_q^{inc} = \begin{pmatrix} \boldsymbol{\Phi}_{\boldsymbol{q}_1}^+ & \mathbf{0} \\ \mathbf{0} & \boldsymbol{\Phi}_{\boldsymbol{q}_2}^+ \end{pmatrix} \quad \boldsymbol{\Phi}_q^{ref} = \begin{pmatrix} \boldsymbol{\Phi}_{\boldsymbol{q}_1}^- & \mathbf{0} \\ \mathbf{0} & \boldsymbol{\Phi}_{\boldsymbol{q}_2}^- \end{pmatrix} \quad \boldsymbol{\Phi}_f^{inc} = \begin{pmatrix} \boldsymbol{\Phi}_{\boldsymbol{f}_1}^+ & \mathbf{0} \\ \mathbf{0} & \boldsymbol{\Phi}_{\boldsymbol{f}_2}^+ \end{pmatrix} \quad \boldsymbol{\Phi}_f^{ref} = \begin{pmatrix} \boldsymbol{\Phi}_{\boldsymbol{f}_1}^- & \mathbf{0} \\ \mathbf{0} & \boldsymbol{\Phi}_{\boldsymbol{f}_2}^- \end{pmatrix} \tag{15}$$

By implementing the continuity and force equilibrium conditions, the nodal DOFs and forces at the interfaces are equal to those of the undamaged waveguides on each side, i.e.

$$\begin{pmatrix} \boldsymbol{q}_l^c \\ \boldsymbol{q}_r^c \end{pmatrix} = \begin{pmatrix} \boldsymbol{q}_r^1 \\ \boldsymbol{q}_l^2 \end{pmatrix} \quad \begin{pmatrix} \boldsymbol{f}_l^c \\ \boldsymbol{f}_r^c \end{pmatrix} = \begin{pmatrix} \boldsymbol{f}_r^1 \\ \boldsymbol{f}_l^2 \end{pmatrix} \tag{16}$$

The scattering matrix $\mathbf{S}$ is defined as

$$\begin{pmatrix} \boldsymbol{a}^+ \\ \boldsymbol{b}^- \end{pmatrix} = \mathbf{S} \begin{pmatrix} \boldsymbol{a}^- \\ \boldsymbol{b}^+ \end{pmatrix} \tag{17}$$

By combining Equations 13 to 16, then

$$\mathbf{S} = -(-\mathbf{D}_c^* \boldsymbol{\Phi}_q^{ref} + \boldsymbol{\Phi}_f^{ref})^{-1}(-\mathbf{D}_c^* \boldsymbol{\Phi}_q^{inc} + \boldsymbol{\Phi}_f^{inc}) \tag{18}$$

The scattering matrix $\mathbf{S}$ is a block matrix where the diagonal matrices comprise the reflection coefficients, and the off-diagonal matrices contain the transmission coefficients. In these models, reflection coefficients of the damaged section are of interest. Once again, if a reduced number of waves is retained, then the matrix to be inverted in Equation 18 is not square and pseudo-inversion is required [9]. However, since the inversion of this matrix can cause ill conditioning errors, appropriate use of the left eigenvector matrix $\boldsymbol{\Psi}$ from Equation 7 and the orthogonality condition from Equation 8 can eliminate these numerical errors. As a result, one can premultiply Equation 18 by matrix $\boldsymbol{\Psi}_q^{ref}$ defined as

$$\boldsymbol{\Psi}_q^{ref} = \begin{bmatrix} \boldsymbol{\Psi}_{\boldsymbol{q}_1}^- & \mathbf{0} \\ \mathbf{0} & \boldsymbol{\Psi}_{\boldsymbol{q}_2}^- \end{bmatrix} \tag{19}$$

Subsequently, the scattering matrix $\mathbf{S}$ becomes

$$\mathbf{S} = -\boldsymbol{\Psi}_q^{ref}(-\mathbf{D}_c^* \boldsymbol{\Phi}_q^{ref} + \boldsymbol{\Phi}_f^{ref})^{-1} \boldsymbol{\Psi}_q^{ref}(-\mathbf{D}_c^* \boldsymbol{\Phi}_q^{inc} + \boldsymbol{\Phi}_f^{inc}) \tag{20}$$

6 Numerical results

For both RC and prestressed RC models, the undamaged section is modelled similarly to the previous part in WFE. The damaged part is modelled in ANSYS of dimensions and properties similar to the one modelled in WFE previously of total length equal to 0.05 m. The damage is modelled as a diameter reduction over a specific length to simulate the pitting corrosion effect of the reinforcement. $\mathbf{S}$ is calculated at each frequency

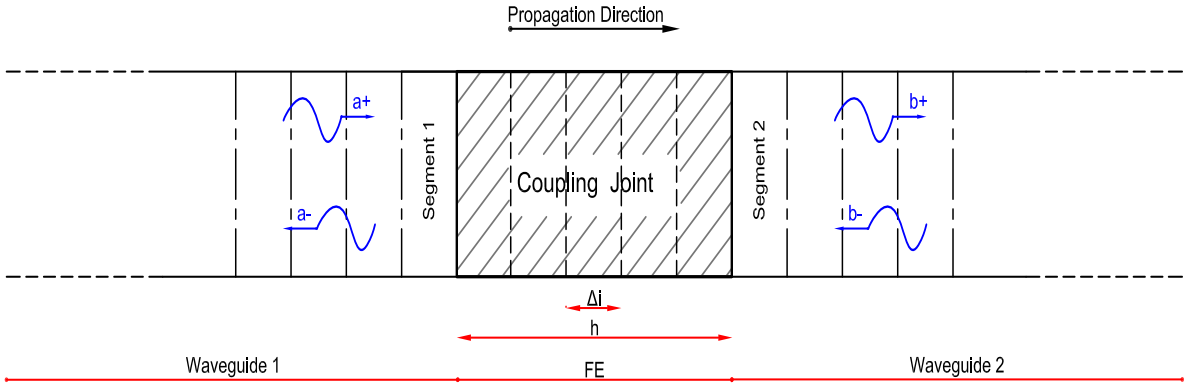

Figure 7: The interface between wave finite elements (segments 1 and 2) connected to a finite element model of the coupling joint discontinuity

step of 50 Hz within the frequency range of 1 to 15 kHz. The next step is to eliminate the high-attenuated modes that have a high imaginary part of the wavenumber. Subsequently, the magnitudes of the reflection coefficients for the least attenuated modes due to damage are plotted in Figures 8 and 9 for RC and prestressed RC respectively. One would expect that the decrease in the diameter of the rebar results in an increase in the magnitude of the reflection coefficients. That is why only the smallest detectable damage is modelled for each model respectively.

It can be seen that the high magnitudes of the reflection coefficients for the least attenuated modes are associated with evanescent and complex modes at their cut-on frequencies. Zero order modes (modes 1-4) show negligible magnitudes for the reflection coefficients due to damage. Consequently, higher order modes have shown sensitivity to loss of area occurring in the steel reinforcements over a specific length. This sensitivity is highlighted by their reflection coefficients due to damage at the mode cut-on frequencies. Furthermore, the normalised nodal displacement in X, Y and Z directions can be plotted in order to identify the corresponding deformed shape for each wave mode. These nodal displacement in the dominant directions are plotted in Figure 10 for prestressed RC. It can be seen that each mode has a dominant displacement in one of the directions Y and Z at their cut-on frequencies.

As shown in Figures 8 and 9, one can notice that similar modes are sensitive to damage in RC and pre-stressed RC models. The magnitudes of the reflection coefficients for the least attenuated modes are slightly higher in prestressed RC than conventional RC for the same damage extent. In addition, the majority of the nodal displacements for the least attenuated modes with high magnitudes of the reflection coefficients due to damage are in Y and Z directions. In addition, the maximum displacement is located at the corners of the cross section of the beam. In practice, the challenge is to pick out the displacement of the defined mode from all other modes excited at this particular cut-on frequency. Identification of the wave modes that are strongly reflected gives a possibility for defining a damage criterion associated with the measurement of corner displacements in the Y and Z directions.

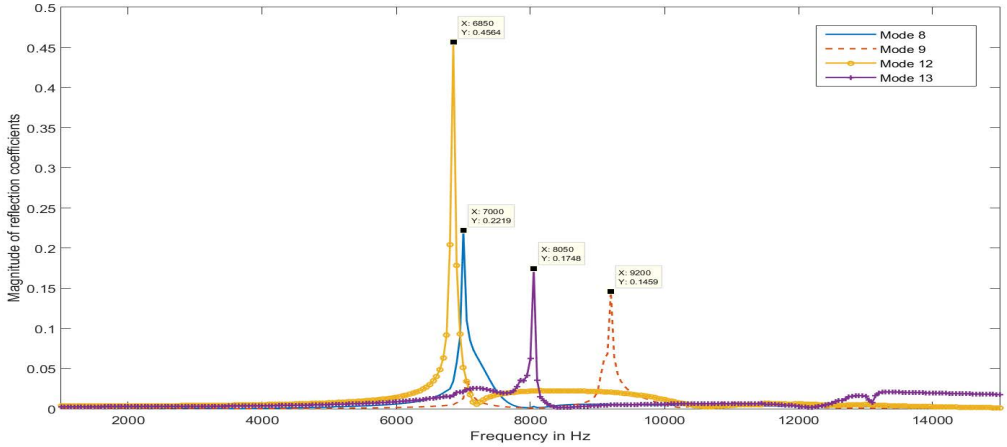

Figure 8: Magnitude of the reflection coefficients for the least attenuated modes in RC due to damage in one rebar: 60 percent diameter reduction over a length of 0.05 m

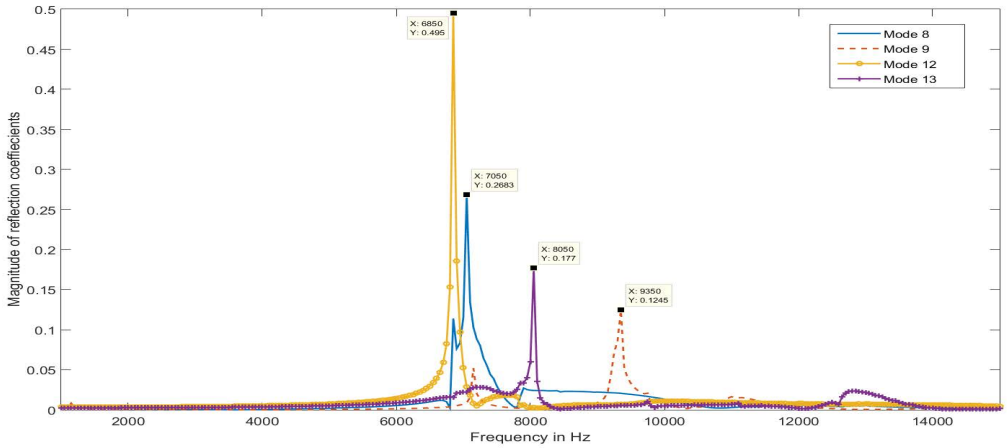

Figure 9: Magnitude of the reflection coefficients for the least attenuated modes in prestressed RC due to damage in one rebar: 60 percent diameter reduction over a length of 0.05 m

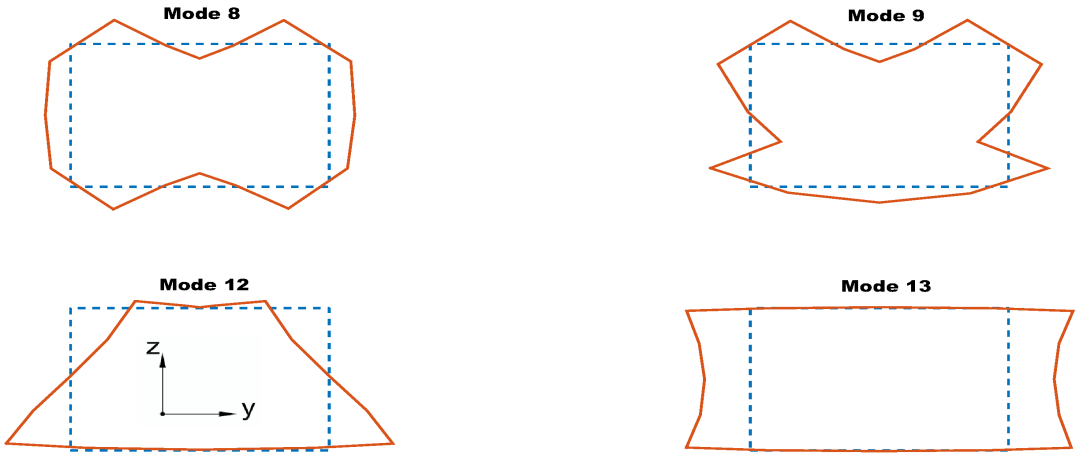

Figure 10: Nodal displacements in Y and Z directions for the least attenuated modes that are most strongly reflected due to rebar area reduction of 60 percent in prestressed RC: Deformed section (—), Undeformed section (- - -)

7 Conclusions

In order to extract wave characteristics in reinforced concrete with and without prestress, the WFE has been applied to a reinforced deep concrete beam section for both damaged and undamaged waveguides. The damaged section is modelled as a reduction of the cross sectional area of the rebar representing the extent of the damage. The prestress effect is modelled as an initial strain value associated with the tension force in the steel reinforcement. Dispersion curves and mode shapes are plotted for the least attenuated waves for prestressed RC. Then, coupling between damaged and undamaged waveguides was developed via the hybrid FE/WFE method. The scattering matrix was formulated, and the reflection coefficients associated with the damaged section were computed. Higher order modes have showed higher sensitivity to potential damage of the reinforcement rebar at their cut-on frequencies and could be considered for further study and practical application. In addition, the majority of the nodal displacements for the least attenuated modes having high magnitudes of the reflection coefficients due to damage are in Y and Z directions where the maximum displacement occurs at the corners of the cross section of the beam.

References

[1] J.M. Renno, B.R Mace, *On the forced response of waveguides using the wave and finite element method*, Journal of Sound and Vibration, Vol. 329,(2010), pp. 5474-5488.

[2] D. Duhamel, B.R Mace, M.J. Brennan, *Finite element analysis of the vibrations of waveguides and periodic structures*, Journal of Sound and Vibration, Vol. 294,(2006), pp. 205-220.

[3] B.R Mace, D. Duhamel, M.J. Brennan, L. Hinke, *Finite element prediction of wave motion in structural waveguides*, Journal of the Acoustical Society of America, Vol. 117,(2005), pp. 2835-2843.

[4] J.M Mencik, M.N. Ichchou, *Wave finite elements in guided elastodynamics with internal fluid*, International Journal of Solids and Structures, Vol. 44,(2007), pp. 2148-2167.

[5] Y. Waki, B.R Mace, M.J. Brennan, *Free and forced vibrations of a tyre using a wave/finite element approach*, Journal of Sound and Vibration, Vol. 323,(2009), pp. 737-756.

[6] Y. Waki, B.R Mace, M.J. Brennan, *Numerical issues concerning the wave and finite element method for free and forced vibrations of waveguides*, Journal of Sound and Vibration, Vol. 327,(2009), pp. 92-108.

[7] J.M. Renno, B.R Mace, *Calculating the forced response of two-dimensional homogeneous media using the wave and finite element method*, Journal of Sound and Vibration, Vol. 330,(2011), pp. 5913-5927.

[8] W.J. Zhou, M.N. Ichchou, O. Bareille, *Finite element techniques for calculations of wave modes in one-dimensional structural waveguides*, Structural Control and Health Monitoring, Vol. 18,(2011), pp. 737-751.

[9] J.M. Renno, B.R Mace, *Calculation of reflection and transmission coefficients of joints using a hybrid finite element/wave and finite element approach*, Journal of Sound and Vibration, Vol. 332,(2013), pp. 2149-2164.

[10] M.N. Ichchou, J.M. Mencik, W. Zhou, *Wave finite elements for low and mid-frequency description of coupled structures with damage*, Computer Methods in Applied Mechanics and Engineering, Vol. 198,(2009), pp. 1311-1326.

[11] W.J. Zhou, M.N. Ichchou, *Wave scattering by local defect in structural waveguide through wave finite element method*, Structural Health Monitoring, Vol. 10,(2010), pp. 335-349.

[12] W.J. Zhou, M.N. Ichchou, *Wave propagation in mechanical waveguide with curved members using wave finite element solution*, Computer Methods in Applied Mechanics and Engineering, Vol. 199,(2010), pp. 2099-2109.

[13] M. Kharrat, W.J. Zhou, O. Bareille, M.N. Ichchou, *Identification and sizing of defects in pipelines by the wave finite element method using torsional guided waves, COMPDYN 2011, ECCOMAS Thematic Conference on Computational Methods in Structural Dynamics and Earthquake Engineering, Corfu, Greece,*(2011).

[14] M. Kharrat, M.N. Ichchou, O. Bareille, W.J. Zhou, *Pipeline Inspection Using a Torsional Guided-Waves Inspection System. Part 2: Defect Sizing by the Wave Finite Element Method*, International Journal of Applied Mechanics, Vol. 06,(2014), pp. 1450035.

[15] A. Kessentini, M. Taktak, M.A. Ben Souf, O. Bareille, M.N. Ichchou, M. Haddar, *Computation of the scattering matrix of guided acoustical propagation by the Wave Finite Element approach*, Applied Acoustics in Multiphysic Systems, Vol. 108,(2016), pp. 92-100.

[16] ANSYS Inc., *ANSYS Mechanical APDL Element Reference*, Release 15.0,(2013).

[17] E.J. O'Brien, A.S. Dixon, *Reinforced and prestressed concrete design: The complete process*, Harlow, England, Longman Scientific and Technical (1995) .